Atmospheric Research 217 (2019) 73–80

Contents lists available at ScienceDirect

Atmospheric Research

journal homepage: www.elsevier.com/locate/atmosres

Characteristics of trace metal concentration and stable isotopic composition of hydrogen and oxygen in "urban-induced heavy rainfall" in downtown Tokyo, Japan; The implication of mineral/dust particles on the formation of summer heavy rainfall

Ryunosuke Uchiyama*, Hiroshi Okochi*, Hiroko Ogata, Naoya Katsumi, Takanori Nakano

Graduate School of Creative Science and Engineering, Waseda University, Okubo 3-4-1, Shinjuku-ku, Tokyo 169-8555, Japan

ARTICLE INFO

Keywords:
Heavy rain
Urban heat island
Air pollutants
Mineral/road dust particle
Ice nuclei
Giant cloud condensation nuclei

ABSTRACT

To investigate the impact of mineral/road dust particles on the formation of sudden and locally distributed heavy rain in urban areas (hereafter, urban-induced heavy rain: UHR), we analyzed the trace metal elements and the stable isotope composition of hydrogen and oxygen in rainwater. Rainwater samples, which were collected in Shinjuku (Japan) from April 2014 to December 2015, were analyzed for 12 trace metal elements (Al, V, Cr, Mn, Fe, Ni, Cu, Zn, Cd, Pb, Se, and As) in three fractions: coarse suspended particles (> 1.2 μm, CSP), acid-insoluble fine suspended particles (0.45–1.2 μm), and a dissolved/acid-soluble fine suspended fraction. Concentrations and wet deposition fluxes of trace metal elements in CSP were markedly higher in UHR than other types of rainfall, i.e., normal rain, typhoon heavy rain, and frontal heavy rain. There were strong positive correlations between $\delta^{18}O$ and the total concentration of trace metal elements in UHR (r = 0.902) and specifically for Fe, Mn, Al, V, and Pb in CSP (r = 0.919, 0.883, 0.823, 0.843, and 0.820, respectively). These findings indicate that mineral/road dust particles were removed by in-cloud scavenging process under the meteorological conditions causing UHR. There is one possibility that they could play important roles as giant cloud condensation nuclei and/or effective ice nuclei for the formation of UHR.

1. Introduction

The occurrence of urban-induced heavy rainfall (hereafter, UHR) has been observed in many urban areas throughout the world in the previous 50 years (Changnon Jr., 1968; Atkinson, 1971; Jauregui and Romales, 1996; Mikami et al., 2005; Goswami et al., 2006; Dou et al., 2015). The quantity of UHR can cause severe flood disaster because the rainfall amount can exceed the capacity of sewage systems and drainage canals (Kawasaki and Meguro, 2011). The Japanese media refer to UHR events as "guerrilla rainstorms" because predicting the formation of UHR is very difficult. Forecasting UHR is problematic because of the following two characteristics: its sudden occurrence and its local distribution. Typically, a period of UHR persists for only several tens of minutes from its formation (Mikami et al., 2005); therefore, there is little time to take measures to minimize the effects of urban flooding damage caused by the extreme rainfall. As UHR is a locally distributed phenomenon (Mikami et al., 2005), it is very difficult to predict UHR formation based on meteorological analyses using current observation systems and simulation models. Thus, to minimize the damage associated with UHR, it is very important to clarify the formation mechanism of UHR to improve its predictability.

The urban heat island (UHI) phenomenon has been considered as a cause of increased summer heavy rain events (Shiraki et al., 2009; Mikami et al., 2005; Fowler and Hennessy, 1995; Rajeevan et al., 2008) because it causes ascending air currents and accelerated formation of cumulonimbus clouds that can lead to localized heavy rainfall (Fujibe, 2004; Mikami et al., 2005). In addition to the meteorological effects of UHIs, Uchiyama et al. (2017a, 2017b) highlighted the chemical effects of UHIs on the formation of UHR, based on their observations of the chemical components and stable isotopes of hydrogen and oxygen in UHR. They found that UHR had the highest concentrations of acidic components (i.e., H^+, NH_4^+, NO_3^-, and nss-SO_4^{2-}) compared with other types of rain event. They considered that UHIs could accelerate the secondary formation of hygroscopic aerosols (e.g., NH_4NO_3,

* Corresponding authors at: Department of Resources and Environmental Engineering, School of Creative and Engineering, Waseda University, Okubo 3-4-1, Shinjuku-ku, Tokyo 169-8555, Japan.

E-mail addresses: k-u.ryunosuke@suou.waseda.jp (R. Uchiyama), hokochi@waseda.jp (H. Okochi).

https://doi.org/10.1016/j.atmosres.2018.10.017
Received 30 May 2018; Received in revised form 22 September 2018; Accepted 24 October 2018
Available online 02 November 2018

NH_4HSO_4, and $(NH_4)_2SO_4$) because of the high temperature and the accumulation of air pollutants in the ascending air. These secondary aerosols could contribute to the formation of convective clouds as effective cloud condensation nuclei (CCN), scavenged by the developing UHR event. However, these secondary aerosols generally serve as small CCN, making many small cloud droplets that might reduce the overall precipitation efficiency (Rosenfeld and Woodley, 2000).

One possible mechanism for the formation of UHR, suggested by Uchiyama et al. (2017a, 2017b), is the inclusion of giant CCN (> 2 μm) such as sea salts at the base of convective clouds containing many smaller droplets formed by secondary aerosols. The inclusion of giant CCN would accelerate coalescence between the cloud droplets and lead to rapid formation of raindrop embryos, especially significant in continental clouds (Levin et al., 2005). This process is called warm rain formation. Another possible mechanism for the formation of UHR is ice nucleation, called cold rain formation, which can be divided into homogeneous and heterogeneous ice nucleation. In situ measurements by aircraft in the deep convective clouds that cause heavy rainfall have revealed that most of the condensed water remains in liquid form down to −37.5 °C, whereas at a slightly lower temperature only ice was found, suggesting homogenous freezing (Rosenfeld and Woodley, 2000). It has long been known that ice crystals will grow preferentially and lead to the rapid formation of precipitable particles under the coexistence of ice crystals and supercooled droplets within a cloud (Hobbs and Rangno, 1985). Braham (1964) reported that ice pellet concentration was unrelated to ground-level ice nuclei (IN) concentration and that the pellets were formed via homogeneous freezing of drops within convective clouds, which is a process that causes summer rain showers in central USA.

Mineral dust aerosols can play important roles in heterogeneous freezing by acting as effective IN (Atkinson et al., 2013) but they can also affect cloud water chemistry. Based on satellite observations and in situ measurements, it has been suggested that desert dust acting as IN might suppress precipitation (Rosenfeld et al., 2001). Simulations have also shown that allowing mineral dust particles to act as efficient IN reduces the amount of rain on the ground compared with a case in which they are inactive (Levin et al., 2005). When dust particles are active as both giant CCN and effective IN, continental clouds become wider. Some trace metal ions such as iron and manganese, dissolved from dust particles into cloud droplets, have long been known as important aqueous-phase catalysts in sulfite oxidation. Recently, this process has been revealed the dominant in-cloud oxidation pathway (Harris et al., 2013). After evaporation of cloud droplets, the remaining sulfate-coated coarse dust particles can serve as giant CCN (Wurzler et al., 2000). In Amazonian clouds at temperatures warmer than −25 °C, ice formation is dominated by primary biological aerosols, such as plant fragments or fungal spores (Prenni et al., 2009), which can have considerable influence on the evolution of clouds and precipitation. At temperatures colder than −25 °C, both locally emitted primary biological aerosols and mineral dust aerosols from the Saharan Desert can act as IN and induce cold rain formation (Prenni et al., 2009). However, the contribution of dust particles to the formation of sudden and locally distributed heavy rain in urban areas remains uncertain.

The objective of this study was to investigate the impact on UHR formation of airborne dust particles, probably dispersed from paved roads and building rooftops in urban areas by the strong updrafts associated with daytime UHIs in summer. Trace metal elements within the UHR were examined to derive information on the IN, e.g., mineral/road dust particles, although major inorganic ions such as sulfate, nitrate, and sodium ions provided information on the CCN (Uchiyama et al., 2017b). Here, we report the concentration distributions of soluble and insoluble forms of trace metals, their wet deposition fluxes, and the relationships of their fractions with the oxygen isotope in UHR in comparison with other types of rain event.

2. Method

2.1. Sampling site and method

Rainwater samples were collected on the rooftop of a building (ca. 65 m) in the Nishi-Waseda campus (35.7°N, 139.7°E), Waseda University, which is located in Shinjuku, Japan. The 97 rainwater samples were obtained on an event basis from April 2014 to December 2015. The samples were collected using a filtering-type collector (Funakura et al., 2007) equipped with polycarbonate filter holder (Sartorius D-3400, diameter: 80 mm), membrane filter (Millipore RAWP04700, pore diameter: 1.2 μm), and polypropylene bottle (volume: 3 L). To prevent adsorption to the inside wall of the bottle and sedimentation of trace metal elements in the collected rainwater, HNO_3 (pH = 2) was added into the polypropylene bottle in advance. The polypropylene bottle was placed inside a Styrofoam cooler box to block out sunlight and prevent evaporation of the samples (Funakura et al., 2007), although the rainwater was collected as soon as possible after each rain event.

2.2. Analytical method

After collection, the rainwater samples were filtered with a membrane filter (pore size: 0.45 μm) to remove any particulate matter as soon as possible. The filtrates were stored in clean polypropylene bottles in a refrigerator at 4 °C until used in chemical and stable isotopic analyses. The membrane filters (pore diameter: 1.2 μm) used in the filtering-type collectors were also placed in a polypropylene petri dish and dried in a desiccator as coarse suspended particles (> 1.2 μm) until chemical analysis. The filters used for the filtration were also placed in a polypropylene petri dish and dried in a desiccator as acid-insoluble fine suspended particles (0.45–1.2 μm in diameter) until chemical analysis. Both coarse and fine suspended particles on the filters were decomposed by microwave-assisted acid digestion using 8 mL mixed acid solution of concentrated HNO_3 (special grade chemical, KANTO CHEMICAL CO., INC) and 0.01 M H_2O_2 (FUJIFILM Wako Pure Chemical Corporation) (HNO_3:H_2O_2 = 7:1). Table S1 shows the program of microwave-assisted acid digestion. We visually checked that suspended particles were completely decomposed after the end of the microwave-assisted acid digestion. To prepare the samples for analysis, a 100-fold dilution was made with ultrapure water for the decomposed solution of the suspended particles and a 5-fold dilution was prepared for the acid dissolved fraction. All samples were spiked with 1 mg/L In as an internal standard. Twelve trace metals (Al, V, Cr, Mn, Fe, Ni, Cu, Zn, Cd, Pb, Se, and As) were analyzed by inductively coupled plasma mass spectrometry (Agilent Technology, 7700×). The detection limits of each trace metal were 0.139 μg/L for Al, 0.811 ng/L for V, 4.50 ng/L for Cr, 4.18 ng/L for Mn, 15.5 ng/L for Fe, 13.3 ng/L for Ni, 3.33 ng/L for Cu, 31.9 ng/L for Zn, 1.03 ng/L for Cd, 0.646 ng/L for Pb, 6.74 ng/L for Se, and 6.51 ng/L for As. The concentration of each trace metal in both coarse and fine suspended particle fractions was calculated by substituting the filter blank from the analytical values and then dividing them by the volume of the collected rainwater. The concentration data sets were authorized by Smirnov-Grubbs test. The sampling and analytical methods used for the stable isotope compositions of hydrogen (δD) and oxygen ($\delta^{18}O$) in the rainwater were the same as in Uchiyama et al. (2017b).

2.3. Classification of rainwater samples

According to the Japan Meteorological Agency (JMA), heavy rain is defined as > 30 mm of rain in an hour. However, as UHR usually stops within an hour, we defined heavy rain as an event with rainfall intensity of > 5 mm/10 min, using the 10-min rainfall data from the JMA to classify the rain events. For the classification, we consulted the two nearest JMA observatories: Tokyo station (35.7°N, 139.8°E; ~25 m) and

Nerima station (35.7°N, 139.6°E; ~51 m). We also defined normal rain as an event with a 10-min rainfall amount of < 5 mm. In addition, we classified heavy rain events into three types based on their formation process: 1) frontal heavy rain (FHR), i.e., heavy rain caused by a front; 2) typhoon heavy rain (THR), i.e., heavy rain caused by a typhoon; and 3) UHR, i.e., sudden and locally distributed heavy rain caused by neither a front nor a typhoon. Heavy rain was distinguished based on meteorological charts with 180-min intervals and the infra-red satellite (HIMAWARI-7/8) images with 60-min intervals obtained from the Japan Weather Association. The procedure of heavy rain classification was as follows.

a. When heavy rain occurred, we consulted the meteorological charts and classified heavy rain associated with a typhoon as THR.
b. If the heavy rain was not caused by a typhoon, we used the infra-red imagery to check whether the rain was caused by large-scale precipitation clouds developed around the symbol of the cold, warm front, and stationary fronts. Heavy rain caused by a front was classified as FHR.
c. If the heavy rain was not caused by either a typhoon or a front, it was regarded as UHR.

Examples of the meteorological charts and weather camera imagery used for the identification of the three types of heavy rain can be found in Uchiyama et al. (2017a).

For this study, we classified the 97 rainwater samples as follows: 86 normal rain samples, 5 UHR samples, 4 THR samples, and 2 FHR samples.

3. Results and discussion

3.1. Concentration of trace metal elements in various types of rainwater and their sources

Table 1 shows the mean concentrations of trace metal elements in rainwater in the three fractions: coarse suspended particles (> 1.2 μm; hereafter, CSP), acid-insoluble fine suspended particles (0.45–1.2 μm; hereafter, AIF), and a dissolved and acid-soluble fine suspended fraction (hereafter, DAS). No trace of Cr was detected in CSP in any of the rain events. The total concentrations of the sum of trace metals in UHR (605 μg/L; $n = 5$) and FHR (694 μg/L; $n = 2$) were > 1.7 times higher than normal rain (351 μg/L; $n = 86$), but the total concentration in THR (141 μg/L; $n = 5$) was one half that of normal rain. UHR had the highest concentration of the sum of trace metals in CSP (391 μg/L; $n = 5$), which was 3.2 times higher than normal rain (121 μg/L; $n = 86$). However, UHR had the second lowest concentration of the sum of trace metals in DAS (98.0 μg/L; n = 5), which was followed by THR (67.2 μg/L; $n = 2$). Many trace metals (except Al, Fe, and Cr) in the DAS fraction accounted for > 65% of the total concentration in the samples of the various types of rain event, except for UHR. The solubility of each trace metal depends on the type of airborne aerosol particles scavenged by cloud droplets/raindrops, the lifetimes of the cloud droplets/raindrops, and the acidity of rainwater pH. The rainwater pH in UHR was found lower than in other types of rain event (see Table 1 in Uchiyama et al., 2017b), and the lifetimes of the cloud droplets/raindrops were found shortest in UHR (see rainfall time in Fig. 1). These results suggest that UHR effectively scavenges airborne insoluble coarse particles, probably such as mineral/road dust particles, which act as effective IN, and/or that the concentrations of such airborne coarse particles and acidic substances were high just before the UHR event (Uchiyama et al., 2017b).

It was found that Al, Fe, and Zn were the dominant trace metals measured in all types of rain event (i.e., 96.4% of the total concentration of trace metals in normal rain, 97.4% in UHR, 97.3% in THR, and 96.7% in FHR), while the other trace metals (i.e., V, Cr, Mn, Ni, Cu, Cd, Pb, Se, and As) constituted subcomponents. Furthermore, Fe and Al had the highest concentrations in CSP in UHR. The concentrations of Al and Fe in UHR were 2.6 and 3.6 times higher, respectively, than in normal rain. It is known that Al is an indicator of soil/mineral particles (Fujimura and Hashimoto, 1977), while Fe and Mn in SPM are components derived primarily from road dust (Arai et al., 1982). Shiraishi et al. (2002) reported the concentrations of seven heavy metals in road dust collected from three main streets of Tokyo in July, which is a time when UHR events frequently occur. They found the mean concentrations of Zn (240 μg/g; $n = 10$), Cu (210 μg/g; n = 10), Pb (97 μg/g; n = 10), and Cd (0.35 μg/g; n = 10) in the road dust were higher than in the Earth's crust. Conversely, the mean concentrations of Fe (21,000 μg/g; n = 10) and Mn (400 μg/g; n = 10) in the road dust were lower than in the Earth's crust. The ratios of the total concentration of four trace metals (i.e., Cu, Pb, Cd, and Mn but not Zn) to that of Fe (Mn/Fe: 0.019, Cu/Fe: 0.019, Pb/Fe: 0.0038, Cd/Fe: 3.2×10^{-5}) in UHR were similar to road dust (Mn/Fe: 0.019, Cu/Fe: 0.010, Pb/Fe: 0.0042, Cd/Fe: 1.7×10^{-5}). This suggests the trace metals (except Zn) in UHR originated primarily from road dust particles. Interestingly, the same concentration ratios in other types of rain event were different to road dust (i.e., Mn/Fe: 0.013, Cu/Fe: 0.005, Pb/Fe: 0.0023, and Cd/Fe: 1.9×10^{-4} in normal rain; Mn/Fe: 0.025, Cu/Fe: 0.022, Pb/Fe: 0.0032, and Cd/Fe: 7.1×10^{-4} in THR; and Mn/Fe: 0.034, Cu/Fe: 0.018, Pb/Fe: 0.0087, and Cd/Fe: 5.4×10^{-4} in FHR). Very strong correlations were found between the total concentrations of Fe and Mn ($r = 0.983$), Fe and V ($r = 0.991$), and Mn and V ($r = 0.998$) in CSP in UHR (see Fig. SI-1), and a p values < .01 were considered statistically significant for all of them, which suggests that their main source was probably road dust particles.

The Zn/Fe ratios in all types of rain event (0.20 in normal rain, 0.44 in UHR, 0.55 in THR, and 0.58 in FHR) were much higher than in road dust (0.024), indicating that the total concentration of Zn in UHR was affected by other sources. Saito et al. (2012) collected airborne aerosol particles in the range of 7 nm to 10 μm from the rooftop of a five-story building (22 m) located very close to our sampling site. They reported the number concentration of airborne aerosol particles and the concentrations of 18 metal elements in the particles, and they performed correlation analyses of the size distributions and monthly variations of the trace metals. They established that soil contributed most of the metals (mainly Fe, Ca, and Mg) contained in particles > 1 μm, while incineration fly ash contributed most of those (i.e., Pb, As, Cd, Cu, Sb, Mn, K, and Zn) found in particles < 1 μm. It was reported that Zn was present mainly in airborne aerosol particles in the range 0.3–0.8 μm and that its concentration was high during September–January (Saito et al., 2012). Another possible source of Zn other than incineration fly ash in urban areas is vehicle emissions (Arai et al., 1982; Kasahara, 1996).

3.2. Comparison of wet deposition flux of total trace metals in normal rain, UHR, THR, and FHR

The wet deposition fluxes of the total trace metals in normal rain ($n = 86$), UHR ($n = 5$), THR ($n = 4$), and FHR ($n = 2$) are shown in Fig. 1, together with the rainfall time per event and hourly mean rainfall amount from April 2014 to December 2015. The group “Others” shown in Fig. 1 means the subcomponents of the trace metals. The average rainfall times of normal rain, UHR, THR, and FHR were 14.1, 1.58, 15.3, and 12.3 h, respectively. The hourly mean rainfall amounts, calculated by dividing the rainfall amount by the rainfall time, of normal rain, UHR, THR, and FHR were 1.91, 12.3, 8.46, and 3.25 mm/h, respectively. UHR had the shortest duration (i.e., < 2 h) and the greatest intensity (i.e., > 10 mm/h), although the sample number was inadequate. The wet deposition flux of the total trace metals in UHR was 11.1 times higher than normal rain, 6.25 times higher than THR, and 3.29 times higher than FHR. UHR had the second highest total concentration of trace metals, as shown in Table 1, but it had the highest wet deposition flux because of the extremely high hourly mean rainfall amount.

Table 1
Mean concentration and standard deviation of trace metal elements in rainwater from April 2014 to December 2015 in Shinjuku. Values in parentheses are contribution of the concentration of trace metals in each fraction to total concentration. Values > 50% are shown in bold.

	Al	V	Cr	Mn	Fe	Ni
	Concentration (μg/L) ± S.D.					
Dissolved/acid soluble						
Normal (n = 86)	32.2 ± 134 (31)	0.45 ± 1.01 (**72**)	0.16 ± 0.54 (46)	3.16 ± 6.16 (**69**)	22.0 ± 54.5 (17)	0.69 ± 8.47 (**74**)
UHR (n = 5)	12.1 ± 3.47 (7.6)	0.63 ± 0.45 (**58**)	0.03 ± 0.04 (14)	2.24 ± 0.89 (37)	12.9 ± 5.31 (4.1)	0.52 ± 0.25 (43)
THR (n = 4)	26.5 ± 8.09 (**54**)	0.17 ± 0.08 (**71**)	0.03 ± 0.04 (27)	0.91 ± 0.75 (**65**)	10.8 15.9] (19)	0.41 ± 0.53 (**89**)
FHR (n = 2)	59.3 ± 51.5 (31)	1.02 ± 0.63 (**73**)	0.24 ± 0.25 (34)	7.41 ± 6.45 (**72**)	37.7 ± 28.6 (12)	1.11 ± 0.52 (**80**)
Acid insoluble						
Normal (n = 86)	33.1 ± 79.4 (32)	0.07 ± 0.32 (11)	0.19 ± 0.41 (**54**)	0.44 ± 0.81 (10)	42.2 ± 79.4 (32)	0.08 ± 0.85 (8.2)
UHR (n = 5)	44.7 ± 15.3 (28)	0.13 ± 0.05 (12)	0.18 ± 0.10 (**86**)	0.69 ± 0.18 (11)	65.5 ± 15.8 (21)	0.31 ± 0.73 (26)
THR (n = 4)	14.6 ± 22.1 (30)	0.04 ± 0.05 (17)	0.08 ± 0.12 (**73**)	0.21 ± 0.32 (15)	24.8 ± 36.4 (44)	0.03 ± 0.05 (6.5)
FHR (n = 2)	92.3 ± 41.0 (49)	0.23 ± 0.09 (16)	0.47 ± 0.22 (**66**)	1.65 ± 0.91 (16)	157 ± 85.1 (51)	0.20 ± 0.08 (14)
Coarse particle						
Normal (n = 86)	39.3 ± 146 (38)	0.11 ± 0.59 (17)	LOD	0.99 ± 4.69 (21)	66.2 ± 291 (**51**)	0.17 ± 1.67 (18)
UHR (n = 5)	102 ± 108 (**64**)	0.33 ± 0.28 (30)	LOD	3.16 ± 2.74 (**52**)	238 ± 201 (**75**)	0.38 ± 0.40 (31)
THR (n = 4)	8.38 ± 8.86 (17)	0.03 ± 0.03 (12)	LOD	0.28 ± 0.27 (20)	21.0 ± 20.7 (37)	0.02 ± 0.03 (4.3)
FHR (n = 2)	37.0 ± 10.2 (20)	0.14 ± 0.01 (10)	LOD	1.23 ± 0.17 (12)	111 ± 12.8 (36)	0.07 ± 0.04 (5.1)
Total						
Normal (n = 86)	105 ± 272	0.63 ± 1.75	0.35 ± 0.73	4.59 ± 8.67	130 ± 342	0.94 ± 9.25
UHR (n = 5)	158 ± 46.4	1.09 ± 114	0.21 ± 0.59	6.09 ± 0.12	317 ± 3.59	1.21 ± 1.99
THR (n = 4)	49.5 ± 17.6	0.23 ± 13.2	0.10 ± 0.07	1.41 ± 0.08	56.6 ± 0.57	0.45 ± 28.0
FHR (n = 2)	189 ± 150	1.39 ± 72.6	0.71 ± 0.51	10.3 ± 0.33	306 ± 5.33	1.38 ± 89.5

	Cu	Zn	Cd	Pb	Se	As	Σ
	Concentration (μg/L) ± S.D.						
Dissolved/acid soluble							
Normal (n = 86)	4.40 ± 16.9 (**87**)	89.2 ± 179 (**86**)	0.06 ± 0.22 (**88**)	0.48 ± 0.80 (**67**)	0.10 ± 0.31 (**86**)	0.28 ± 1.34 (**91**)	153 ± 279 (44)
UHR (n = 5)	2.25 ± 0.73 (38)	66.9 ± 41.2 (**59**)	0.01 ± 0.02	0.39 ± 0.49 (33)	0.05 ± 0.08 (**83**)	0.08 ± 0.05 (**73**)	98.0 ± 46.4 (16)
THR (n = 4)	1.17 ± 0.84 (**94**)	26.9 ± 21.2 (**87**)	0.03 ± 0.02	0.13 ± 0.32 (**72**)	0.01 ± 0.01	0.10 ± 0.10 (**77**)	67.2 ± 35.2 (48)
FHR (n = 2)	5.28 ± 4.11 (**95**)	146 ± 117 (**83**)	0.16 ± 0.17	2.42 ± 2.38 (**91**)	0.17 ± 0.18	0.25 ± 0.21 (**83**)	262 ± 212 (38)
Acid insoluble							
Normal (n = 86)	0.46 ± 1.39 (9.0)	0.50 ± 1.52 (0.5)	LOD	0.05 ± 0.35 (6.4)	0.01 ± 0.03 (8.3)	0.01 ± 0.07 (3.4)	77.0 ± 141 (22)
UHR (n = 5)	1.74 ± 3.18 (29)	2.88 ± 3.97 (2.5)	LOD	0.17 ± 0.15 (14)	LOD	0.02 ± 0.02 (18)	116 ± 26.5 (19)

(*continued on next page*)

Table 1 (*continued*)

	Cu	Zn	Cd	Pb	Se	As	Σ
	Concentration (μg/L) ± S.D.						
THR (n = 4)	0.07 ± 0.05 (5.6)	0.22 ± 0.31 (0.7)	LOD	0.01 ± 0.02 (5.6)	LOD	LOD	40.0 ± 58.9 (28)
FHR (n = 2)	0.29 ± 0.07 (5.2)	2.71 ± 0.34 (1.5)	LOD	0.07 ± 0.02 (2.6)	LOD	0.04 ± 0.02 (13)	255 ± 127 (37)
Coarse particle							
Normal (n = 86)	0.21 ± 0.67 (4.2)	14.1 ± 128 (14)	0.01 ± 0.14 (9.5)	0.19 ± 1.19 (27)	0.01 ± 0.07 (5.4)	0.02 ± 0.23 (5.7)	121 ± 531 (35)
UHR (n = 5)	1.99 ± 4.24 (33)	44.3 ± 34.2 (39)	LOD	0.64 ± 0.63 **(53)**	0.01 ± 0.02 (17)	0.01 ± 0.03 (9.1)	391 ± 323 **(65)**
THR (n = 4)	LOD	3.81 ± 4.11 (12)	LOD	0.04 ± 0.06 (22)	LOD	0.03 ± 0.04 (23)	33.6 ± 29.2 (24)
FHR (n = 2)	LOD	27.8 ± 5.73 (16)	LOD	0.16 ± 0.08 (6.0)	LOD	0.01 ± 0.02 (3.3)	178 ± 17.4 (26)
Total							
Normal (n = 86)	5.07 ± 17.0	104 ± 229	0.07 ± 0.35	0.72 ± 1.49	0.12 ± 0.34	0.31 ± 1.47	351 ± 770
UHR (n = 5)	5.98 ± 1.06	114 ± 7.58	0.01 ± 71.0	1.21 ± 0.02	0.06 ± 0.87	0.12 ± 0.10	605 ± 337
THR (n = 4)	1.24 ± 0.29	31.0 ± 0.45	0.04 ± 11.6	0.18 ± 0.01	0.01 ± 0.17	0.13 ± 0.03	141 ± 105
FHR (n = 2)	5.57 ± 0.45	177 ± 2.95	0.16 ± 78.5	2.66 ± 0.12	0.17 ± 1.61	0.30 ± 0.13	694 ± 357

The occurrence of UHR is limited to summer (June–September). Therefore, the differences in the concentrations and the composition of trace metals between UHR and the other types of rain event could be due to seasonal variation. The seasonal variation of the wet deposition flux of the total trace metals is shown in Fig. 2, together with their distributions in each fraction, i.e., CSP, AIF, and DAS in normal rain (spring: $n = 17$, summer: $n = 29$, autumn: n = 29, and winter: $n = 11$). The wet deposition flux of the total trace metals in normal rain was highest because of the high hourly rainfall amount in summer. The distribution of the total trace metals in DAS was highest in summer, which suggests the highest distribution of the total trace metals in CSP in UHR was not due to seasonality but to other factors. One possible factor is the suspension of insoluble coarse particles dispersed from paved roads and building rooftops to the upper air by strong updrafts associated with daytime UHIs in summer, just before the occurrence of UHR.

3.3. Characteristics of wet deposition flux of trace metals in UHR

The wet deposition flux of each trace metal and its distribution in UHR are shown in Fig. 3. The wet deposition flux of the trace metals in decreasing order was Fe (3.89 $mg/m^2/h$) > Al (1.95 $mg/m^2/h$) > Zn (1.40 $mg/m^2/h$) > > Mn (74.9 $\mu g/m^2/h$) and Cu (73.5 $\mu g/m^2/h$) > Ni (14.9 $\mu g/m^2/h$), Pb (14.8 $\mu g/m^2/h$), and V (13.4 $\mu g/m^2/h$) > > Cr (2520 $ng/m^2/h$), As (1420 $ng/m^2/h$), Se (708 $ng/m^2/h$), and Cd (134 $ng/m^2/h$). It was found that Fe, Al, Mn, and Pb were present mainly in CSP (75%, 64%, 52%, and 53%, respectively), while Zn, V, As, Se, and Cd were present mainly in DAS (59%, 58%, 73%, 83%, and 86%, respectively). These results indicate that large quantities of insoluble coarse particles were scavenged effectively by UHR. The results also showed that Cr was present mainly in AIF and that the distributions of Fe, Al, Mn, Cu, and Ni were reasonably high in AIF.

3.4. Relationship between $\delta^{18}O$ and the concentration of trace metals in normal rain and UHR

3.4.1. $\delta^{18}O$ vs. the concentration of trace metals in each fraction in normal rain and UHR

Uchiyama et al. (2017b) suggested that $\delta^{18}O$ in UHR could be an indicator of the distance from the sampling point to the area of UHR formation (or of the time from UHR formation to the collection of the rainwater). Their results showed that there was a high negative correlation ($r = -0.962$) between $\delta^{18}O$ and the distances from the sampling point to the formation area of UHR within 10 km (for 5 samples). Heavier stable isotopes of water (^{18}O, D) condense and precipitate faster than lighter ones (^{16}O, H) according to Rayleigh equation. That is the reason of this high negative correlation between $\delta^{18}O$ and the distances. The chemical components in UHR, which have high correlation with $\delta^{18}O$, could be gathered at the point of UHR formation by wind convergence, flung up to the upper air by heat emissions created by UHIs, or scavenged during the initial stage of a UHR event (Uchiyama et al., 2017b). The relationships between $\delta^{18}O$ and the total concentrations of trace metals in normal rain and UHR are shown in Fig. 4. Although the sample number was inadequate, strong positive correlation was found in UHR ($r = 0.902$; $p < .05$), suggesting that airborne aerosol particles including trace metal elements were scavenged by in-cloud processes. Conversely, only weak correlation was found in normal rain ($r = 0.366$).

The relationship between $\delta^{18}O$ and the contribution of trace metals in DAS, which was defined as the ratio of the concentration of trace metals in DAS to the total concentration of trace metals in UHR, is shown in Fig. 5. Strong negative correlation was found between $\delta^{18}O$ and the contribution of the trace metals in DAS in UHR ($r = -0.807$; $p < .1$), suggesting that trace metals in the scavenged coarse particles could be dissolved during the initial stage (the highest $\delta^{18}O$ sample) of a UHR event.

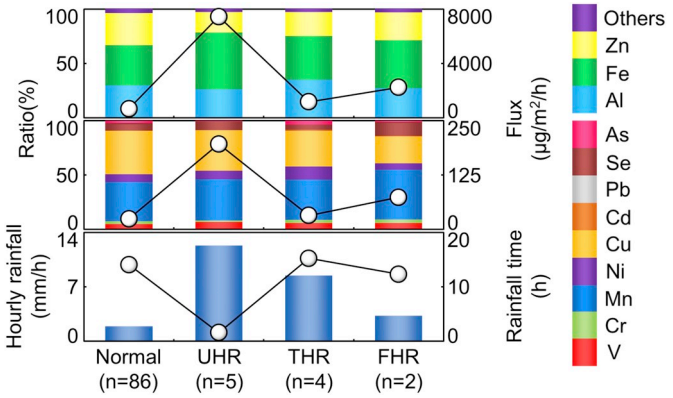

Fig. 1. The upper (a) and middle (b) and bottom (c) panels show deposition fluxes of the total concentration of the trace metals and rainfall intensity/duration in normal rain, UHR, THR, FHR, respectively. The white circles in the upper panel indicate the total wet deposition flux of all trace metal element, in middle panel indicate the total wet deposition flux of subcomponents ("others" in the upper panel), and in the bottom panel indicates mean rainfall time of each rainfall event.

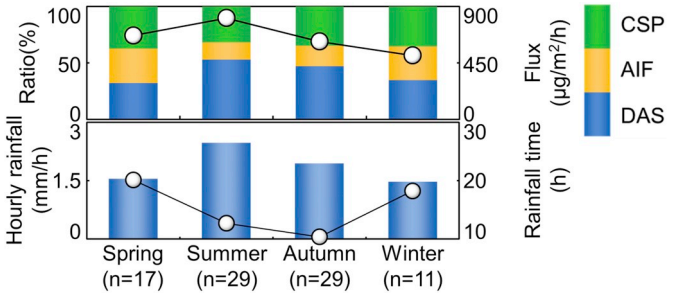

Fig. 2. Seasonal change of the wet deposition flux of total trace metals and the distribution of the three fractions, i.e., dissolved/acid-soluble fraction (DAS), acid-insoluble fine suspended particles (AIF), and coarse suspended particles (CSP) in normal rain, together with the rainfall time (line graph in the bottom column) and hourly mean rainfall amount (bar graph in the bottom column).

3.4.2. $\delta^{18}O$ vs. the concentration of each trace metal in UHR

The relationships between $\delta^{18}O$ and the total concentration of each trace metal in UHR are shown in Fig. 6. Strong positive correlations were found between $\delta^{18}O$ and the total concentration of Al, Fe, Mn, and Pb in UHR ($r > 0.80, p < .05$), although there were only five samples. No trace metal had stronger correlation between $\delta^{18}O$ and their

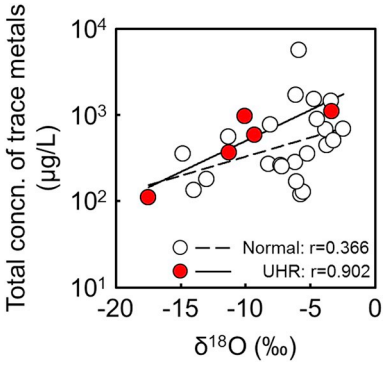

Fig. 4. Relationship between $\delta^{18}O$ and total concentration of trace metals in normal rain (white circle) and UHR (red circle).

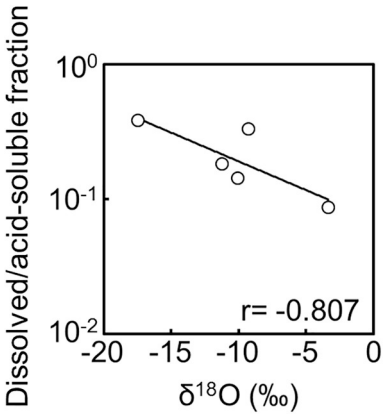

Fig. 5. Relationship between $\delta^{18}O$ and the contribution of dissolved/acid-soluble trace metals to total concentration of trace metals in UHR.

concentration in each of the three fractions, i.e., CSP, AIF, and DAS, than between $\delta^{18}O$ and the total concentration (see Fig. SI-2). However, we found the correlation coefficients between $\delta^{18}O$ and the concentration of each trace metal in CSP (Al: $r = 0.785$, Fe: $r = 0.896$, Zn: $r = 0.827$, Mn: $r = 0.840$, V: $r = 0.845$, Ni: $r = 0.641$, and Pb: $r = 0.745$) were higher than in AIF and DAS. As discussed in section 3.1, Fe, Mn, Pb, Cu, and Cd are typically found in road dust. These results indicate that road dust particles could have been gathered at the point of UHR formation by wind convergence, flung up to the upper air via updrafts due to heat emissions created by a UHI, and scavenged

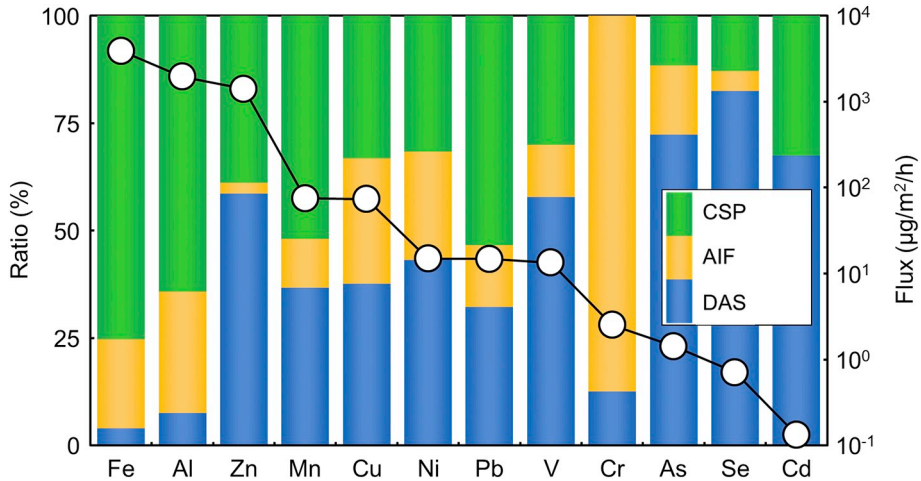

Fig. 3. Wet deposition flux of each trace metal and the distribution of three fractions, i.e., dissolved/acid-soluble fraction (DAS), acid-insoluble fine suspended particles (AIF), and coarse suspended particles (CSP) in UHR.

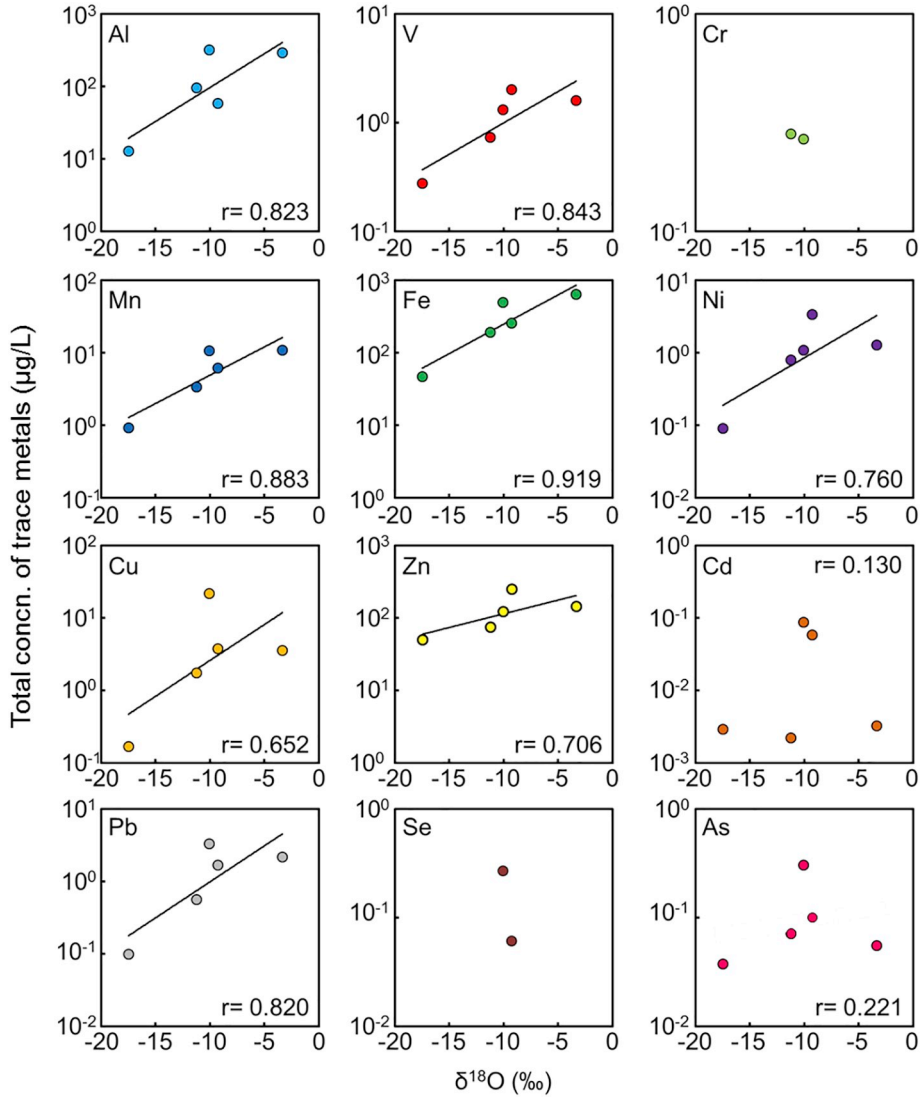

Fig. 6. Relationships between $\delta^{18}O$ and total concentration of each trace metal in UHR. Only two values are plotted for Cr and Se because the other three samples had their concentrations below the detection limit.

during the initial stage of a UHR event (Uchiyama et al., 2017b).

4. Conclusions

Based on the analysis of this study, the following four conclusions were derived.

1) UHR had the highest total concentration of the sum of trace metals in CSP (391 μg/L; $n = 5$) among all types of rain event, which was 3.2 times higher than normal rain (121 μg/L; $n = 86$). Furthermore, Fe, Al, and Zn accounted for > 96% of the total concentration of the sum of the trace metals in all types of rain event.
2) The concentration of the sum of trace metals in CSP in UHR (65% of the total concentration) was higher than in other types of rainfall (35% in normal rain, 24% in THR, and 26% in FHR). Moreover, Fe, Al, Pb, and Mn in UHR were present mainly in CSP (75.3%, 64.1%, 53.4%, and 51.9% of the total concentration of each trace metal, respectively), which were possibly derived from mineral/road dust.
3) UHR had the highest wet deposition flux of the sum of trace metals in the three fractions (7.44 mg/m^2/h) because of the high hourly mean rainfall amount, which was 11.1 times higher than normal rain (672 μg/m^2/h).
4) The strongest correlations between $\delta^{18}O$ and the total concentrations of Al, Fe, Mn, V, and Pb in the three fractions in UHR (Al: $r = 0.823$, Fe: $r = 0.919$, Mn: $r = 0.883$, V: $r = 0.843$, Pb: $r = 820$, p value < .05) indicated that coarse particles, derived primarily from mineral/road dust, were gathered at the point of UHR formation by wind convergence, flung up to the upper air by updrafts associated with a UHI, and removed by in-cloud scavenging process. There is one possibility that they are scavenged as giant cloud condensation nuclei and/or effective ice nuclei during the initial stage of a UHR event although further research is needed.

Acknowledgments

This research was partly supported by the Nippon Life Insurance Foundation, Japan and Asahi Group Foundation, Japan. The study was conducted with the support of a Joint Research Grant for Environmental Isotope Study from the Research Institute for Humanity and Nature, Japan. We thank James Buxton MSc from Edanz Group (www.edanzediting.com./ac) for editing a draft of this manuscript.

Appendix A. Supplementary data

Supplementary data to this article can be found online at https://doi.org/10.1016/j.atmosres.2018.10.017.

References

Arai, H., Watanabe, Y., Ohta, M., Suzuki, M., Hirano, K., Yoneyama, E., 1982. A study on air pollution caused by automobile exhaust gas in areas along a road (rep. 7) - Measurements of suspended particulates in areas along a road. In: Report of research institute of nuisance, Yokohama City. vol. 7. pp. 15–26 (in Japanese).

Atkinson, B.W., 1971. The effect of an urban area on the precipitation from a moving thunderstorm. J. Appl. Meteorol. 10, 47–55.

Atkinson, J.D., Murray, B.J., Woodhouse, M.T., Whale, T.F., Baustian, K.J., Carslaw, K.S., Dobbie, S., Sullivan, D.O., Malkin, T.L., 2013. The importance of feldspar for ice nucleation by mineral dust in mixed-phase clouds. Nature 498, 355–358.

Braham, R.R., 1964. What is the Role of Ice in Summer Rain-Showers? J. Atmos. Sci. 21, 640–645.

Changnon Jr., S.A., 1968. The la Porte weather anomaly – fact or fiction? Bull. Am. Meteorol. Soc. 49, 4–11.

Dou, J., Wang, Y., Bornstein, R., Miao, S., 2015. Observed spatial characteristics of Beijing urban climate impacts on summer thunderstorms. J. Appl. Meteorol. Climatol. 54, 94–105.

Fowler, A.M., Hennessy, K.J., 1995. Potential impacts of global warming on the frequency and magnitude of heavy precipitation. Nat. Hazards 11, 283–303.

Fujibe, F., 2004. Effect of heat island to precipitation: convective precipitation in summer. Tenki 51, 109–115 (in Japanese).

Fujimura, M., Hashimoto, Y., 1977. Estimation of emission sources of trace elements in an atmospheric aerosol by particle size distributions. Nippon Kagaku Kaishi 902–906 (in Japanese).

Funakura, T., Okochi, H., Nagoya, T., Inazu, K., Minami, Y., Igarashi, Y., 2007. Development of Solar-Powered Rainwater Collector and Observation of Wet Deposition Fluxes on the Mountainside of Mt. Fuji, BUNSEKI. KAGAKU 56, 805–811 (in Japanese).

Goswami, B.N., Venugopal, V., Sengupta, D., Madhusoodanan, M.S., Xavier, P.K., 2006. Increasing trend of extreme rain events over India in a warming environment. Science 314, 1442–1445.

Harris, E., Sinha, B., Pinxteren, D., Tilgner, A., Fomba, K.W., Schneider, J., Roth, A., Gnauk, T., Fahlbusch, B., Mertes, S., Lee, T., Collett, K., Foley, S., Borrmann, S., Hoppe, P., Herrmann, H., 2013. Enhanced role of transition metal ion catalysis during in-cloud oxidation of SO_2. Science 340, 727–730.

Hobbs, P.V., Rangno, A.L., 1985. Ice particle concentration in clouds. J. Atmosp. Sci. 42, 2523–2549.

Jauregui, E., Romales, E., 1996. Urban effects on convective precipitation in Mexico city. Atmos. Environ. 30, 3383–3389.

Kasahara, M., 1996. Chemical composition and production mechanisms of atmospheric aerosols. Earozoru Kenkyu 11, 120–126 (in Japanese).

Kawasaki, A., Meguro, K., 2011. A preliminary investigation on the introduction of housing water tanks to store rainwater for improving urban environment and disaster risk reduction. Mon. J. Inst. Ind. Sci., Univ. Tokyo 63, 451–456 (in Japanese).

Levin, Z., Teller, A., Ganor, E., Yin, Y., 2005. On the interactions of mineral dust, sea-salt particles, and clouds: a measurement and modeling study from the Mediterranean Israeli Dust Experiment campaign. J. Geophy. Res. 110 (D20202), 1–19.

Mikami, T., Yamato, H., Ando, H., Yokoyama, H., Yamaguchi, T., Ichino, M., Akiyama, Y., Ishii, K., 2005. Climatological study on the summer intensive heavy rainfall in Tokyo. Ann. Rep. Tokyo Metro. Res. Inst. Environ. Prot. 33–42 (in Japanese).

Prenni, A.J., Petters, M.D., Kreidenweis, S.M., Heald, C.L., Martin, S.T., Artaxo, M., Garland, R.M., Wollny, A.G., Pöschl, U., 2009. Relative roles of biogenic emissions and Saharan dust as ice nuclei in the Amazon basin. Nat. Geo. 2, 402–405.

Rajeevan, M., Bhate, J., Jaswal, A.K., 2008. Analysis of variability and trends of extreme rainfall events over India using 104 years of gridded daily rainfall data. Geophys. Res. Lett. 35, L18707.

Rosenfeld, D., Woodley, W.L., 2000. Deep convective clouds with sustained supercooled liquid water down to −37.5 °C. Nature 405, 440–442.

Rosenfeld, D., Rudich, Y., Lahav, R., 2001. Desert dust suppressing precipitation: a possible desertification feedback loop. Proc. Natl. Acad. Sci. U. S. A. 98, 5975–5980.

Saito, I., Onuki, A., Hosaka, M., Ogata, A., Nakae, D., 2012. Measurement of size distribution and metal content in airborne particle matter. Ann. Rep. Tokyo Metr. Inst. Pub. Health 63, 255–265 (in Japanese).

Shiraishi, S., Wayanabe, I., Kuno, K., 2002. Heavy metal accumulation in the street dust, roadside soil and roadside tree leaves nearby main streets in Tokyo. Jpn. J. Environ. Chem. 12, 829–837 (in Japanese).

Shiraki, Y., Higuchi, A., Kondo, A., 2009. The effect of an urban environment on the precipitation in areas around Tokyo. Environ. Sci. 22, 187–195 (in Japanese).

Uchiyama, R., Okochi, H., Katsumi, N., Ogata, H., 2017a. The impacts of air pollutants to the formation of “Urban-induced heavy rainfall (UHR)” in downtown Tokyo, Japan. J. Geophys. Res. https://doi.org/10.1002/2017JD026803.

Uchiyama, R., Okochi, H., Ogata, H., Katsumi, N., Asai, D., Nakano, T., 2017b. Geochemical and stable isotope characteristics of urban heavy rain in the downtown of Tokyo, Japan. Atmos. Res. 194, 109–118.

Wurzler, S., Reisin, T.G., Levin, Z., 2000. Modification of mineral dust particles by cloud processing and subsequent effects on drop size distributions. J. Geophys. Res. 105, 4501–4512.